JMEPEG (2012) 21:128–136
DOI: 10.1007/s11665-010-9798-7

1059-9495/$19.00

Improvement of Electrochemical Surface Properties in Steel Substrates Using a Nanostructured CrN/AlN Multilayer Coating

G. Cabrera, F. Torres, J.C. Caicedo, W. Aperador, C. Amaya, and P. Prieto

(Submitted May 12, 2010; in revised form July 14, 2010)

Improvement of corrosion properties on AISI D3 steel surfaces coated with [CrN/AlN]$_n$ multilayered system deposited for various periods (Λ) via magnetron sputtering has been studied in this work exhaustively. For practical effects compared were the latter properties with CrN and AlN single layers deposited with the same conditions as the multilayered systems. The coatings were characterized in terms of crystal phase; chemical composition, micro-structural, and electrochemical properties by x-ray diffractometry, energy dispersive x-ray, Fourier transforming infrared spectroscopy, atomic force microscopy, scanning electron microscopy, Tafel polarization curves, and electrochemical impedance spectroscopy. Corrosion evolution was observed via optical microscopy. Results from x-ray diffractometry analysis revealed that the crystal structure of [CrN/AlN]$_n$ multilayered coatings has an NaCl-type lattice structure and hexagonal structure (wurtzite-type) for CrN and AlN, respectively, i.e., it was made non-isostructural multilayered. The best behavior was obtained by the multilayered period: Λ = 60 nm (50 bilayers), showing the maximum corrosion resistance (polarization resistance of 1.18 KΩ, and corrosion rate of 1.02 mpy). Those results indicated an improvement of anticorrosive properties, compared to the CrN/AlN multilayer system with 1 bilayer at 98 and 80%, respectively. Furthermore, the corrosion resistance of steel AISI D3 is improved beyond 90%. These improvement effects in multilayered coatings could be attributed to the number of interfaces that act as obstacles for the inward and outward diffusions of ion species, generating an increment in the energy or potential required for translating the corrosive ions across the coating/substrate interface. Moreover, the interface systems affect the means free path on the ions toward the metallic substrate, due to the decreasing of the defects presented in the multilayered coatings.

Keywords coatings structure and morphology, electrochemical properties, magnetron sputtering, multilayered coatings

1. Introduction

The PVD method via magnetron sputtering processes has been used for coating cutting tools since the 1980s. Thus, among the processes used for this purpose, magnetron sputtering and its reactive variants have proven to be very successful. Many studies reported in the literature that coating materials such as TiCN (Ref 1), AlCN (Ref 2), YSZ (Ref 3), CrAlN (Ref 4), $BiMnO_3$ (Ref 5), etc. have been synthesized with high stability; confirm the advantages of the PVD process. Surface engineering of metallic substrates with protective coatings like single-layered hard coatings, such as TiCN, CrN, and AlN, have played an important role a few years ago, due to their mechanical and tribological properties reflected in higher hardness and toughness, as well as in high corrosion resistance compared to steel substrates used in industrial applications (Ref 6). In regards to this first generation coating, the CrN had been used as a protective coating material because of its characteristics such as high melting point, hardness, thermal conductivity, and corrosion resistance, all of this associated to its different crystalline structures (cubic CrN and hexagonal Cr_2N) (Ref 7). Although these properties in the past were enough to guarantee the growth and productivity of different industrial clusters, nowadays, it is not, due to the rise in the production requests which is involved each time, shorter work cycle, high performance with more longevity of the different industrial tools and mechanisms, moreover, without neglect to the environmental demands. In the case of CrN coating, two ways have been proposed to upgrade its properties. The first was based on adding another element into the CrN coating to form either a ternary coating or a composite coating, examples of these are the CrAlN single-layered systems (Ref 4). The second proposed was depositing two kinds of nitride coatings alternately with the purpose of taking advantage of the multilayer or superlattice arrangements, for instance TiN/ZrN (Ref 8), TiCN/TiNbCN (Ref 9), CrN/NbN (Ref 10), and CrN/AlN systems (Ref 11). Properties as corrosion resistance of CrN single layer coatings have been enhanced in the past using NbN by way of CrN/NbN multilayered systems. The enhancement on this property is attributed to the number of interfaces that act as obstacles for the inward and outward diffusions of ion species, which together with the corrosion resistance of the NbN, avoid

G. Cabrera, F. Torres, J.C. Caicedo, C. Amaya, and **P. Prieto**, Department of Physics, Universidad del Valle, Cali, Colombia; **W. Aperador**, Escuela Colombiana de Ingeniería Julio Garavito, Bogotá, Columbia; and **P. Prieto**, Center of Excellence for Novel Materials, Cali, Columbia. Contact e-mail: jcaicedoangulo@gmail.com.

the attack of these ions over the steel substrates, protecting it from catastrophic failure (Ref 12). For the past 7 years, the study of CrN/AlN multilayer coatings has been focused on the development of superlattice structures; because they have shown good results related specifically to the improvement of the mechanical properties and oxidation resistance as compared to CrN single layer coatings applied on cutting tools (Ref 4, 13). With the aim to widen the range of application of multilayer systems, it is necessary to evaluate its stability under corrosive atmospheres. The aim of this work is to evaluate the influences of CrN/AlN multilayer coatings deposited onto steel substrates with different bilayer periods, Λ, and bilayers number, *n*, in their electrochemical nature compared with those of uncoated AISI D3 steel substrates for possible surface applications in processes with aggressive environments (e.g., polymer industry). For this purpose, silicon (100) and AISI D3 steel substrates were coated with CrN/AlN multilayer deposited with bilayer periods (Λ) between 3 μm and 60 nm and bilayers number (*n*) between 1 and 50, via a reactive magnetron sputtering system with a total thickness of 3.0 μm.

2. Experimental Details

CrN/AlN multilayered were deposited on to silicon (100) and AISI D3 steel substrates using a multi-target r.f. magnetron sputtering system, with an r.f. source (13.56 MHz) for the applied voltage bias on the substrate, and Cr and Al targets with 99.9% purity. The coatings were deposited on Si substrates due to the preferential orientation which facilitates the analysis of x-ray diffraction patterns, and has little influence on IR spectra. A 350 W magnetron power was applied to the Cr target, while a power of 400 W was applied to the Al target. The deposition chamber was initially pumped down to less than 5×10^{-6} mbar, using a gas mixture of Ar (92%) + N_2(8%). Used was a bias voltage of −50 V, the substrate temperature was around 250 °C and a substrate to target distance of 7 cm for all coatings. During the deposition, chamber pressure was maintained at 2×10^{-3} mbar. For multilayered depositions, the aluminum and chromium targets were covered periodically with a steel shutter. Before deposition, the targets and substrates were sputter-cleaned during 20 min. The thicknesses ratios of AlN, CrN single-layered, and CrN/AlN multilayered systems were obtained by means of a Dektak 3030 profilometer.

An exhaustive x-ray diffraction (XRD) study was carried out for multilayered and homogeneous coatings in high angled ranges with Bragg-Brentano configurations (θ/2θ) by use of a PANalytical X'Pert PRO diffractometer with Cu Kα radiation (λ = 1.541 Å). High-angled XRD scans permitted characterization of the preferred-orientations related to textured growth. The chemical composition of the single layer coatings was determined by energy dispersive x-ray (EDX) analysis with a high-purity Ge EDX detector for the reliable acquisition of EDX spectra using a Philips XL 30 FEG. Analyses to identify the characteristic bonds at single layer systems were done by Fourier Transformed Infrared spectroscopy (FTIR) using a Shimatzu 8000 (600-3500 cm^{-1}) spectrometer which uses a Nerst ceramic source. Superficial characteristics were determined using an Atomic Force Microscopy (AFM) from Asylum Research MFP-3D® and Phenom FEI Scanning Electron Microscopy (SEM) equipped with an optic light with a magnification range of 525-24.000× and a high sensibility detector (multi-mode) for scattering electrons.

An electrochemical characterization of all coatings was performed using a PC-14 Gamry model system. A three-electrode electrochemical cell was used with a platinum counter electrode and an Ag/AgCl electrode as the reference electrode. The sample to be tested was the working electrode whose surface area exposed to the corrosive medium was of approximately 1 cm^2. All the electrochemical tests were performed in 3.5% NaCl solution prepared with distilled water under free air conditions at room temperature. The sample was cleaned in distilled water before loading on the Teflon sample holder. The sample was kept in the solution for enough time prior to the potentiodynamic polarization study to establish the open-circuit potential (E_{OCP}) or the steady state potential. After getting the stable open-circuit potential the upper and the lower potential limits of linear sweep voltammetry were set at −0.25 up to 0.6 V, with respect to the E_{OCP}, respectively. The sweep rate was 0.5 mV/s. The corrosion potential (E_{corr}) and the corrosion current densities (i_{corr}) were deduced from the Tafel plot (i.e., log *i* vs. *E* plot). Impedance measurements were conducted using a frequency response analyzer. The spectrum was recorded in the frequency range of 10 mHz-100 kHz with a data density of five points per decade. The applied alternating potential had root-mean-square amplitude of 10 mV on the E_{corr}. After each experiment the impedance data was displayed as a Nyquist diagram. The corrosion evolution on surface coatings was analyzed using optical microscopy (Olympus PME-3) and Scanning Electron Microscopy (SEM).

3. Results and Discussion

3.1 Structural and Compositional Analysis of CrN/AlN Multilayered Coatings

Figure 1 shows a typical XRD diffraction pattern of CrN/AlN deposited onto a (100) silicon substrate with Λ = 300 nm and *n* = 10. CrN and AlN layered within the multilayered system were polycrystalline exhibiting diffraction peaks with a preferential orientation (100) corresponding to *w*-AlN phase located at 33.48°, other peaks at 72.40°, 77.50°, and 82.54° corresponding to the planes (201), (004), and (202), respectively, these were attributed to AlN structure. The diffraction peaks at 37.88°, 44.12°, and 64.32° corresponding to the planes (111), (200), and (220), respectively, for CrN cubic structure. The diffraction peaks at 40.84° and 55.54° corresponding to the planes (002) and (112), associated to Cr_2N hexagonal structure (Ref 14-16). These preferential orientations are in agreement with JCPDF 00-025-1133 and JCPDF 00-011-0065 from AlN and CrN ICCD cards, respectively. Regarding the lattice parameter, obtained from the preferential orientation in the AlN and CrN single-layered was as well as was the multilayered system with bilayers number (*n* = 10) and bilayer period (Λ = 30 nm), in this study the Nelson-Riley extrapolation technique was employed in the refinement procedure to determine the value of a_0 and c_0 (±0.0001 nm), because this technique permits direct precision determination of the lattice constant (see Table 1). The results show a compression of the cell unit related to the value reported in the ICCD cards mentioned before for *w*-Al-N (a_0 = 0.311 nm and c_0 = 0.497 nm) and Cr-N (FCC) (a_0 = 0.414 nm), both in powder,

when those were compared with Al-N and Cr-N single-layered coating, and the CrN/AlN multilayered system deposited at r.f. negative bias voltage of −50 V. From the lattice parameter values in Table 1, it is possible to observe that the multilayered system showed a less compressive residual stress than those of single layers, this release stress effect is due to the interfaces which are characteristic of those multilayered systems (Ref 17-19). On the other hand, a careful correction has to be done in all stoichiometric analysis because EDX has low reliability for nitrogen concentration. Therefore, EDX elemental concentrations were obtained using the ZAF correction method; because certain factors related to the sample composition, called matrix effects associated with (atomic number (Z), absorption (A), and fluorescence (F)), can affect the x-ray spectrum produced during the analysis of electron microprobe and therefore, these effects should be corrected to ensure the development of an appropriate analysis. The correction factors for a standard specimen of known compositions were determined initially by the ZAF routine. The relative intensity of the peak K was determined by dead time corrections and a referent correction for the x-ray measured. So, before each quantitative analysis of an EDX spectrum, a manual background correction and an automated ZAF correction was carried out (Ref 8). Thus, Table 1 shows the energy-dispersive x-ray spectroscopy (EDX) values of AlN and CrN single layered, respectively, deposited with an r.f. negative bias voltage of −50 V. All samples were observed via SEM and chemical analyses were done with an amplification of 20000×.

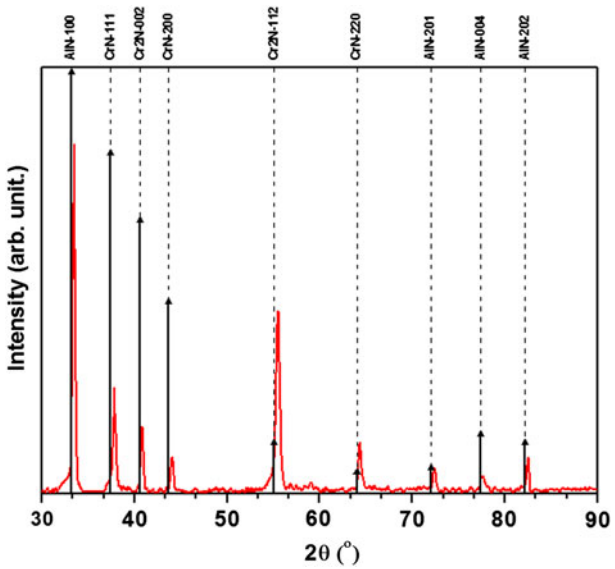

Fig. 1 XRD pattern of the CrN/AlN multilayered coatings with Λ = 300 nm and n = 10

3.2 FTIR Analyses of AlN and CrN Single Layer Coatings

Figure 2(a) shows FTIR transmission spectra of aluminum nitride coatings deposited on Si (100) in the range of 468 to 800 cm^{-1}. After decombolution processes of the band associated to the *wurtzite* (*w*) phase, it was possible to observe the presence of an active mode at 680 cm^{-1} correlated to the *wurtzite* phase of the Al-N (Ref 20, 21), and at 540 cm^{-1} associated to Al-O *stretching* mode (Ref 22). There are five bands around 485, 520, 615, 655, and 691 cm^{-1}, associated to Al-O stretching mode (Ref 23), to the Al-N band of phase unstoichiometric productions (Al_xN_y) (Ref 24), and the last three correspond to different optic modes of the hexagonal AlN (Ref 25-27), respectively.

Figure 2(b) shows FTIR transmission spectra for chromium nitride coatings deposited on Si (100) in the range from 300 to 1150 cm^{-1}. In this result after decombolution processes observed were active modes in the infrared, mainly a narrow band located at 550 cm^{-1} associated to Cr-N bonds. Also noted is an intensive second band located at 450 cm^{-1} correlated to Cr-O bonds associated to the Cr_2O_3 (Ref 28-30). Finally, the authors observed a low intensive band located at 1050 cm^{-1} which could be associated to Cr-N-Cr bonds.

3.3 Surface Analysis

3.3.1 AlN and CrN Single Layered. Atomic Force Microscopy (AFM) was carried out to quantitatively study the surface morphology in all samples. Figure 3 shows 2 × 2 μm images for the AlN (a) and CrN (b), with a *z*-scale around 82.4 ± 2.0 and 18.7 ± 2.0 nm, respectively. From those AFM images, the grain size and roughness values were extracted. For the AlN and CrN coatings growth on steel substrates, the roughness was found to be around 39.01 ± 2.2 and 27.03 ± 2.2 nm, respectively. This roughness difference was found to be crucial in the surface quality of both samples, indicating that AlN grows more disorderly than the CrN coatings under the parameter chosen in this study. A top view of 5 × 5 μm SEM images is presented in Fig 3(c) and (d) for the AlN and CrN coatings, respectively, showing thus, an irregular surface for the AlN coating, corroborated by the AFM images.

3.3.2 CrN/AlN Multilayered. Figure 4 shows 2 × 2 μm images for the n = 10 (a) and n = 50 (b) multilayered systems, with a *z*-scale around 20.4 ± 2.0 and 4.7 ± 1.0 nm, respectively. The grain size and roughness values were found from those AFM images. For the multilayered system with bilayer number n = 10 and n = 50 deposited on steel substrate, the roughness was found to be around 17.80 ± 2.1 and 9.03 ± 2.6 nm, respectively. This roughness difference between the single-layered coatings and the multilayered systems is due to the individual layer thickness in the system

Table 1 Stoichiometric relationship determinate by EDX and lattice parameter of Al-N, Cr-N, and multilayer coatings

Composition from single layered		Lattice parameters from single layered		Lattice parameters from multilayer with n = 10 and Λ = 30 nm	
		Hexagonal *w*-Al_xN_y (100)a_0, nm and c_0, nm	Cubic FCC Cr_xN_y (111)a_0, nm	Hexagonal *w*-Al_xN_y (100)a_0, nm and c_0, nm	Cubic FCC Cr_xN_y (111)a_0, nm
$Al_{68}N_{32}$	$Cr_{65}N_{35}$	0.303 and 0.499	0.410	0.308 and 0.498	0.411

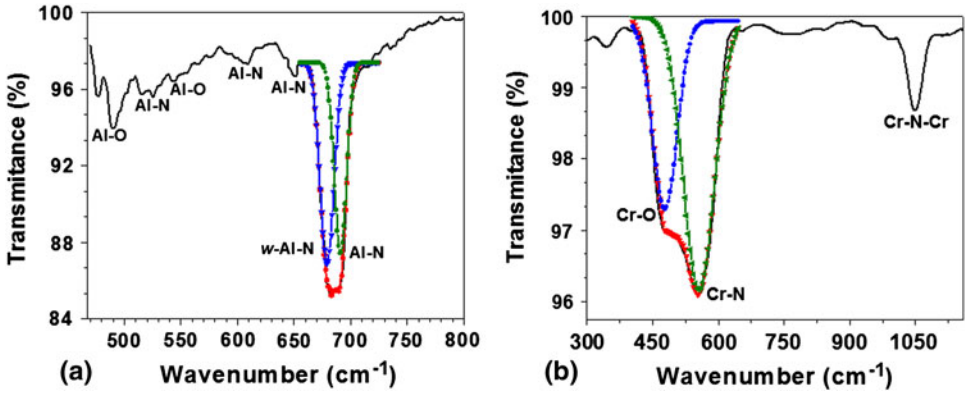

Fig. 2 FTIR spectra of (a) Al-N, (b) Cr-N coatings, deposited with a bias voltage of −50 V on Si (100)

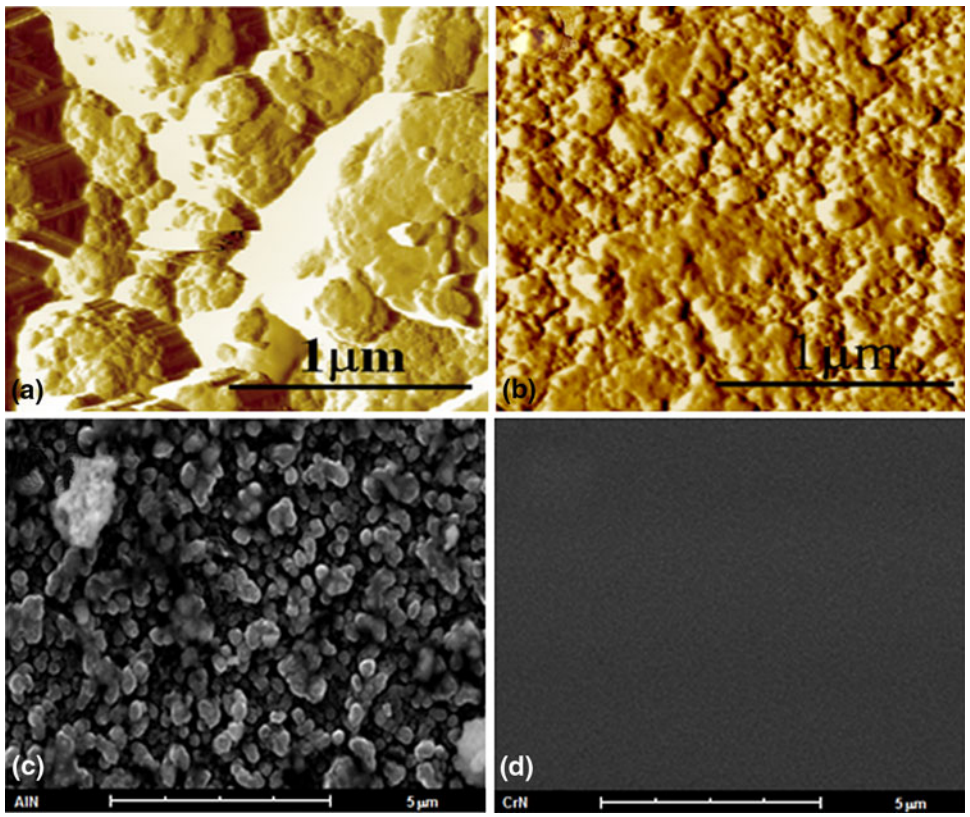

Fig. 3 AFM and SEM images showing morphological surfaces in coatings deposited with a r.f. negative bias voltage of −50 V. AlN (a-c) and CrN (b-d) single layered

being reduced while the bilayer number is increased, generating a coating with lower surface roughness. The latter is important in the estimations on the corrosion behavior of these materials, because a surface with high roughness will generate more corrosion points than a smoother surface. In accordance with the before mentioned, it would be expected that the multilayered system with $n = 50$ shows the best corrosion resistance, even more than the single-layered and the multilayered systems with less bilayers number (n). SEM images (top view) are presented in the Fig. 4(c) and (d) for the CrN/AlN multilayered system with $n = 10$ and $n = 50$, respectively, theses images show a homogeneous surface which confirms those observed by AFM images and EDX analysis. On the other hand, the SEM image in the Fig. 4(e) shows a first glimpse of stack sequences with the AlN and CrN layer within multilayered systems deposited with $\Lambda = 150$ nm ($n = 20$), before of the corrosive process. In this micrograph, exhibited is a broken surface which permits observe the layer slipping over the next layer in a deck type effect. The darkest contrast of AlN layers with respect to CrN ones allowed a clear determination of the layered structures. This difference in color is due to the differences in scattering values for both coatings (Ref 6). The clearest zones of the image correspond to the AISI D3 steel substrate.

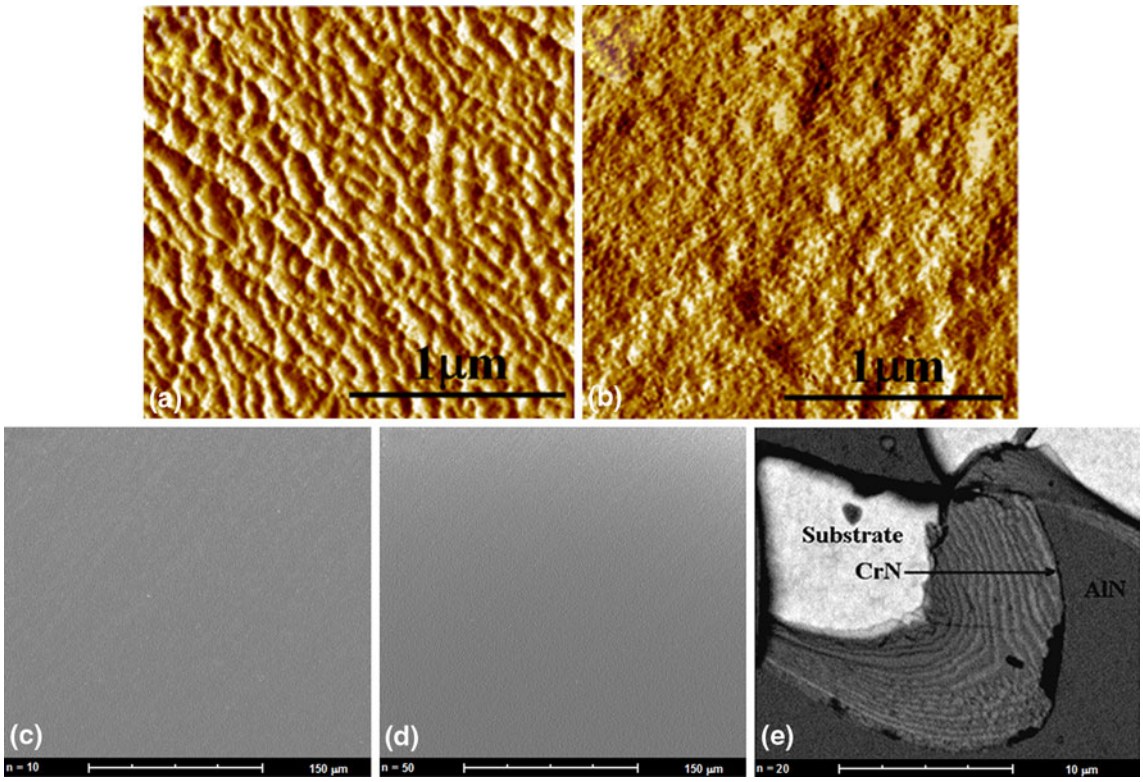

Fig. 4 AFM and SEM images showing morphological surfaces in coatings deposited with a r.f. negative bias voltage of −50 V before of the corrosive process. Multilayered system with (a-c) n = 10, (b-d) n = 50, and (e) n = 20

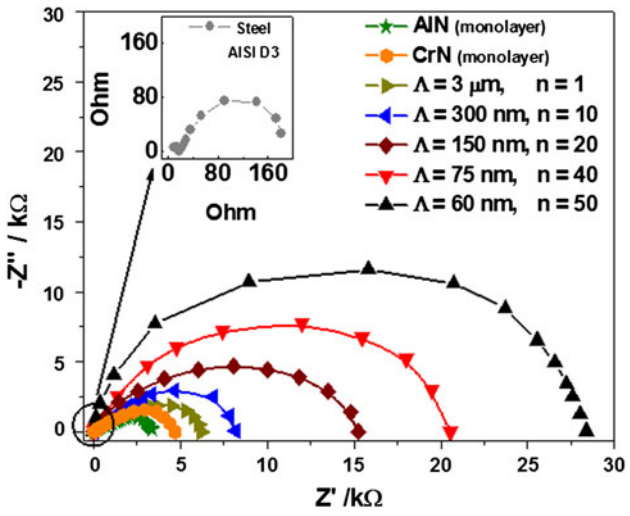

Fig. 5 Impedance diagrams for uncoated and coated steel AISI D3 with AlN and CrN single layered and CrN/AlN multilayered with different bilayer periods (Λ)

3.4 Electrochemical Analyses

Figure 5 shows the Nyquist diagram that corresponds to the uncoated and coated steel AISI D3 substrate with AlN and CrN single layer and CrN/AlN multilayered coatings. To simulate the behavior in the interfaces of all coatings; used was the circuit that corresponds to the Fig. 6 and *Randles* cell for uncoated AISI D3 steel (Ref 31), which indicates that the double-layer capacitance is in parallel with the impedance due to the ions translation reaction (Ref 32). The polarization resistance values increase when the bilayers number is increased. This fact indicates that the mean free path for ions movement across the whole coating is increased as the bilayer period is decreased because the interface number is increased and that the multilayered coating is characterized by a lower porosity with respect to the other single layered. Therefore, the alternated deposition of different thin layers minimizes the presence of an interconnected porosity as is shown in Fig. 10.

For the calculation of the total circuit impedance of Fig. 6, used was the R_1 and R_2 resistances; the value of the solution resistance (R_Ω) was lower in relation to R_1 and R_2 resistances, however, for calculus effect, R_Ω was considered in the fitting of the experimental spectra. The interface solution-multilayer and the double-layer capacitances, CPE_1 and CPE_2, respectively, were used for the calculation of the theory values in the total impedance, which is necessary to diagnose the protection state of the investigated multilayer system. Similar results are reported by Bastidas et al. (Ref 33) and Aperador et al. (Ref 34), which indicates that the CPE_1-R_1 couple, which predominates at high frequencies, may be originated by the passive coating and/or the dielectric properties of the single layer and multilayer systems, while the CPE_2-R_2 couple, controlling at low frequencies, characterizes the corrosion process of the steel/single layer and/or multilayer pore solution interfaces.

On the other hand, Tafel curves of the uncoated and coated steel AISI D3 substrates with AlN, CrN, and CrN/AlN coatings are presented in Fig. 7. These curves allow findings of anodic and cathodic slopes values in each case, which are necessary to calculate a correct value of the corrosion rate for all systems. The corrosion potentials of the coated steel are more

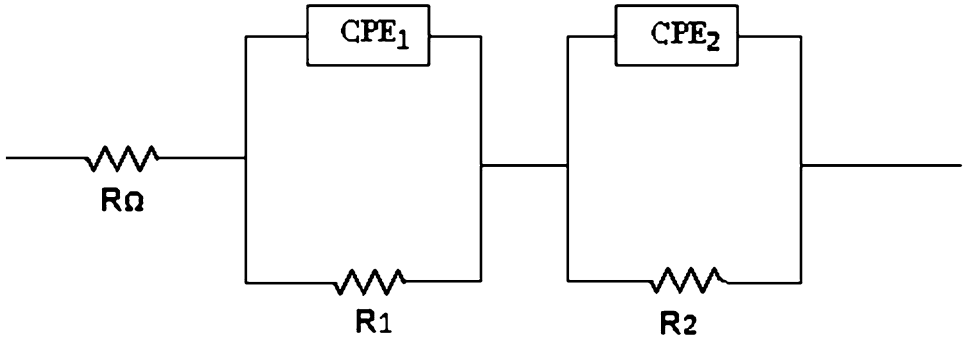

Fig. 6 Electrical equivalent circuit used to fit impedance data of AlN and CrN single layered and CrN/AlN multilayered coatings

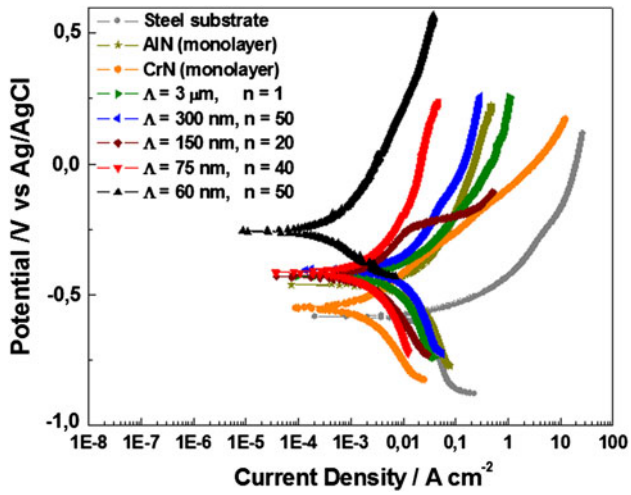

Fig. 7 Tafel curves of the coated and uncoated steel AISI D3 substrates

electropositive when the bilayers number (n) are increased and bilayer period (Λ) is decreased generating more interface numbers than that of the steel bulk material, even if the uncoated steel is compared with the coated steel base on AlN or CrN single layered the corrosion resistance is greater confirming thus, the protective effects of the coatings (Ref 35). The protective corrosion behavior also is characteristic of the multilayer structures with a lattice-mismatch; as a consequence of the increase of the bilayers number (n) and the alternated deposition of different single layered in a same whole coating thickness, which minimizes the presence of an interconnected porosity, decreases the coating roughness surface and increases the coating density. The latter generates an increment in the energy or potential required for moving the corrosive Cl^- ions, across the coating/substrate interfaces. Moreover, the interface systems affect the mean free path on the ions toward the metallic substrate, due to the decreasing of the defects presented in the multilayered coatings (Ref 36).

From Tafel curves in Fig. 7 it is observed that the coated steel for Λ = 3 μm, n = 1 shows the highest downward shift in relation to other multilayer systems, which indicates high corrosion susceptibility in the solution analyzed. The high corrosion susceptibility is associated to the porosities and low interface numbers presented in the bilayer (Ref 37). The polarization resistance values determined by the Nyquist diagrams were used for calculating corrosion rates from the polarization curves, both values are showed in the Table 2. These values clearly show that the corrosion resistance of steel AISI D3 is improved beyond 90% for multilayer effects in coating growths with Λ = 60 nm and n = 50.

3.5 Surface Corrosion Analysis

Optical and scanning electron microscopy analyses were conducted on the coating surfaces immediately after finishing the electrochemical measurements. Optical microscopy images showing the different behaviors of the single-layered and multilayered coatings after following identical electrochemical processes are shows in the Fig. 8(a) h). The images taken under identical conditions of amplification and illumination, clearly display the degradation of the surface due to the NaCl solution chemical attack for the AISI D3 steel substrate uncoated (Fig. 8a), AlN (Fig. 8b), CrN (Fig. 8c) single layer coatings and multilayered systems with Λ = 3 μm, n = 1 (Fig. 8d); Λ = 300 nm, n = 10 (Fig. 8e); Λ = 150 nm, n = 20 (Fig. 8f); Λ = 75 nm, n = 40 (Fig. 8g), and Λ = 60 nm, n = 50 (Fig. 8h) deposited on AISI D3 steel. The degradation levels depended evidently on the type of coating indicating that for this study the multilayer with n = 50 (Λ = 60 nm) is the most appropriate coating to reduce corrosion processes in steel. On the other hand, the damaged regions observed from the SEM images for the systems with n = 10 and n = 50 bilayers (see Fig. 9) in contrast with those before the electrochemical tests (Fig. 4c-d), reveals that the corrosive failure is because of defects at the coatings (e.g., pores, cracks, etc.), which allow the corrosion mechanisms between aggressive environment and the substrate surfaces (Ref 38). From Fig. 9 it is possible to say that the coating with less corrosive damage at the end of the electrochemical test is the system with n = 50 (Λ = 60 nm).

Finally, with the aim to corroborate the observed by optical and SEM images, it was calculated the porosity factor associated to the different coatings in agreement with Tato and Landolt (Ref 39), the porosity factor corresponds to the ratio between polarization resistance of the uncoated substrates and the coated substrates as showed in the next equation:

$$P = \frac{R_{p,u}}{R_{p,r-u}} \quad \text{(Eq 1)}$$

where P is the total coating porosity, $R_{p,u}$ is the polarization resistance of the substrate uncoated and $R_{p,r-u}$ is the measured polarization resistance of coating-substrate system. In Table 2

Table 2 Electrochemical values for uncoated and coated samples

Tech.	Parameter measured	Evaluated system							
					CrN/AlN				
		AISI D3	AlN	CrN	Λ = 3 μm, n = 1	Λ = 300 nm, n = 10	Λ = 150 nm, n = 20	Λ = 75 nm, n = 40	Λ = 60 nm, n = 50
EIS	Polarization resistance, KΩ	9.3×10^{-3}	2.34×10^{-2}	2.54×10^{-2}	2.89×10^{-2}	3.27×10^{-2}	2.55×10^{-1}	1.07	1.18
	Porosity factor, %	…	39	36	32	28	3.6	0.9	0.7
Tafel	Corrosion rate, mpy	10.95	6.28	4.75	5.30	4.05	2.33	1.26	1.02

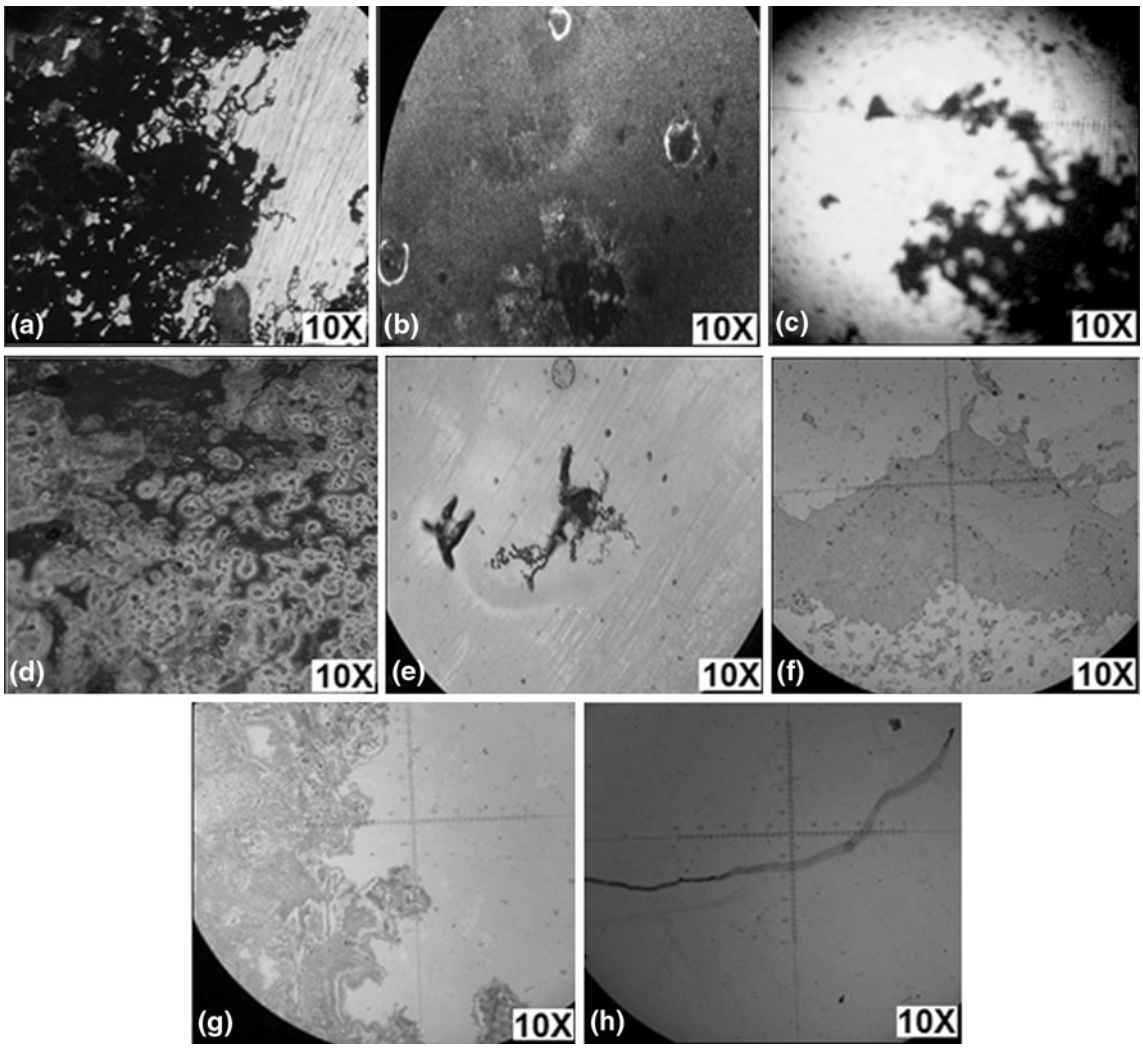

Fig. 8 Optical microscope images at 10× of corrosion processes on (a) AISI D3 steel substrates uncoated, (b) AlN, (c) CrN single-layer coatings and multilayered systems with (d) Λ = 3 μm, n = 1; (e) Λ = 300 nm, n = 10 (f) Λ = 150 nm, n = 20, (g) Λ = 75 nm n = 40 (h) Λ = 60 nm and n = 50 deposited on AISI D3 steel

presented was the porosity factor values obtained, replacing the electrochemical values on the Eq 1 for all coatings. The analysis of porosity factor values applied in all coatings suggests that the porosity factor decreased with the increasing of the bilayers number and decreasing of bilayer period such as is present in Fig. 10. Moreover, these results are in agreement with the optical and SEM images shown in Fig. 8 and 9, respectively.

4. Conclusions

The CrN/AlN multilayer structure was identified to be non-isostructural multilayer of CrN and AlN phases. The preferential orientation for FCC CrN (112) and (100) hexagonal structure (*wurtzite*-type) of AlN was showed via XRD. From FTIR results it was possible to identify the characteristic

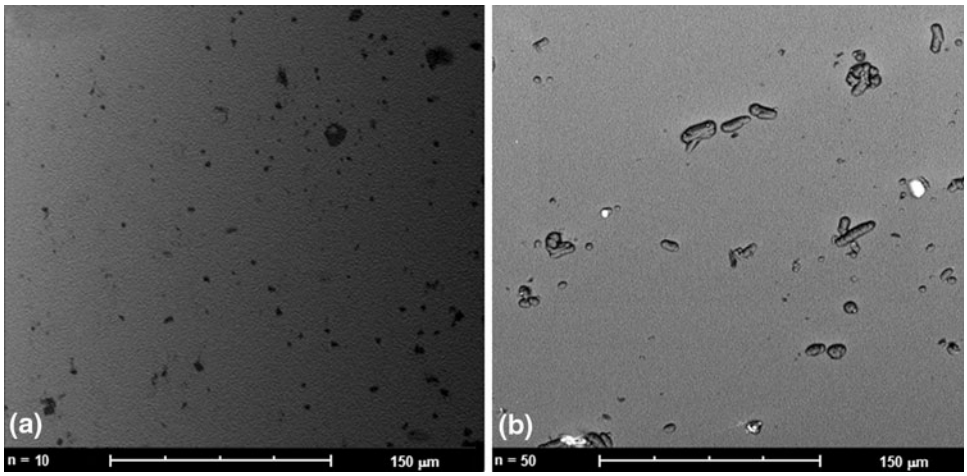

Fig. 9 SEM images of the CrN/AlN coatings after electrochemical tests: (a) system with n = 10 and (b) system with n = 50 bilayered

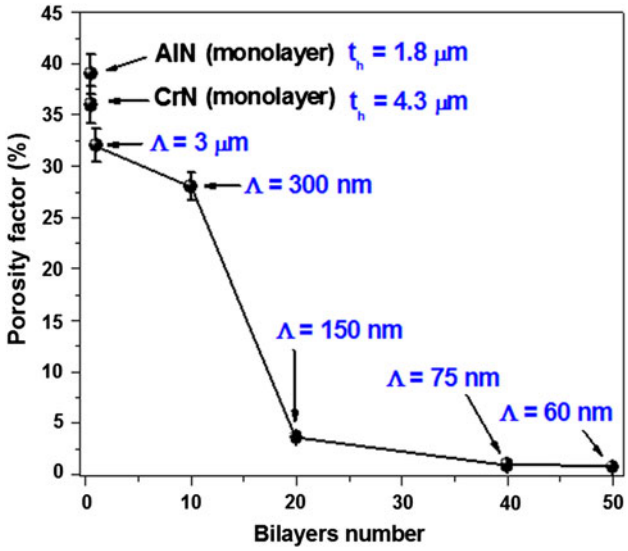

Fig. 10 Correlation between bilayers number and the porosity factor

bonding in both single layer coatings. The morphology and surface characteristics were determined for all coating systems, founding a homogeneous surface for all coatings.

Maximum corrosion resistance was obtained when the bilayer period Λ was 60 nm and the bilayer number was 50 due to the lowest polarization resistance and corrosion rate value, 1.18 KΩ and 1.02 mpy, respectively, which means an increase of around 90% of the surface performance for AISI D3 steel substrates under corrosion processes, such as was presented by Tafel curves. These enhancement effects in the CrN/AlN multilayered coatings could be attributed to the lowest surface roughness corroborated by AFM images and the porosity factor values, this last suggests that the porosity factor decreased with the increasing bilayers number and decreasing of bilayer period. In addition, the increase of the bilayers number (n) and decrease of bilayer period (Λ) with the alternated deposition of different single layered in a same whole coating thickness, not only minimizes the presence of an interconnected porosity in the coatings as was corroborated by optical and SEM analysis, but also increment the energy or potential required for moving the corrosive Cl^- ions across the coating/substrate interfaces, which finally is showed as multilayered systems that exhibit better performance against corrosion.

Acknowledgments

This research was supported by the CDT ASTIN-SENA, Regional Valle, Cali-Colombia, CINVESTAV, Mexico, and the Excellence Center for Novel Materials (CENM) at Universidad del Valle in Colombia under contract RC-043-2005 with Colciencias.

References

1. J.C. Caicedo, C. Amaya, L. Yate, W. Aperador, G. Zambrano, M.E. Gómez, J. Alvarado-Rivera, J. Muñoz-Saldaña, and P. Prieto, Effect of Applied Bias Voltage on Corrosion-Resistance for TiC1-xNx and Ti1-xNbxC1-yNy Coatings, *Appl. Surf. Sci.*, 2010, **256**, p 2876–2883
2. L. Yate, J.C. Caicedo, A. Hurtado Macias, F.J. Espinoza-Beltrán, G. Zambrano, J. Muñoz-Saldaña, and P. Prieto, Composition and Mechanical Properties of AlC, AlN and AlCN Thin Films Obtained by r.f. Magnetron Sputtering, *Surf. Coat. Technol.*, 2009, **203**, p 1904–1907
3. C. Amaya, W. Aperador, J.C. Caicedo, F.J. Espinoza-Beltrán, J. Muñoz-Saldaña, G. Zambrano, and P. Prieto, Corrosion Study of Alumina/Yttria-Stabilized Zirconia (Al_2O_3/YSZ) Nanostructured Thermal Barrier Coatings (TBC) Exposed To High Temperature Treatment, *Corros. Sci.*, 2009, **51**, p 2994–2999
4. J.E. Sanchéz, O.M. Sanchéz, L. Ipaz, W. Aperador, J.C. Caicedo, C. Amaya, M.A. Hernández Landaverde, F. Espinoza Beltran, J. Muñoz-Saldaña, and G. Zambrano, Mechanical, Tribological, and Electrochemical Behavior of Cr1−xAlxN Coatings Deposited by r.f. Reactive Magnetron Co-Sputtering Method, *Appl. Surf. Sci.*, 2010, **256**, p 2380–2387
5. M. Grizalez, E. Martínez, J.C. Caicedo, J. Heiras, and P. Prieto, Occurrence of Ferroelectricity in Epitaxial BiMnO3 Thin Films, *Microelectron. J.*, 2008, **39**, p 1308–1310
6. B.S. Kim, G.S. Kim, S.Y. Lee, and B.Y. Lee, Effects of Al Target Power on the Mechanical and Oxidation Resistance of the CrN/AlN Multilayer Coatings, *Surf. Coat. Technol.*, 2008, **202**, p 5526
7. J.-W. Lee, S.-K. Tien, Y.-C. Kuo, and C.-M. Chen, The Mechanical Properties Evaluation of the CrN Coatings Deposited by the Pulsed DC Reactive Magnetron Sputtering, *Surf. Coat. Technol.*, 2006, **200**, p 3330

8. J.C. Caicedo, C. Amaya, L. Yate, O. Nos, M.E. Gómez, and P. Prieto, Hard Coating Performance Enhancement by Using [Ti/TiN]n, [Zr/ZrN]n and [TiN/ZrN]n Multilayer System, *Mater. Sci. Eng. B*, 2010, **171**, p 56–61
9. J.C. Caicedo, C. Amaya, L. Yate, G. Zambrano, M.E. Gómez, J. Alvarado-Rivera, J. Muñoz-Saldaña, and P. Prieto, TiCN/TiNbCN Multilayer Coatings with Enhanced Mechanical Properties, *Appl. Surf. Sci.*, 2010, **256**, p 5898–5904
10. S.-K. Tien, J.-G. Duh, and J.-W. Lee, Oxidation Behavior of Sputtered CrN/AlN Multilayer Coatings During Heat Treatment, *Surf. Coat. Technol.*, 2007, **201**, p 5138
11. J. Lin, J.J. Moore, B. Mishra, M. Pinkas, X. Zhang, and W.D. Sproul, CrN/AlN Superlattice Coatings Synthesized by Pulsed Closed Field Unbalanced Magnetron Sputtering with Different CrN Layer Thicknesses, *Thin Solid Films*, 2009, **517**, p 5798
12. P.Eh. Hovsepian, D.B. Lewis, W.D. Münz, S.B. Lyon, and M. Tomlinson, Combined Cathodic Arc/Unbalanced Magnetron Grown CrN/NbN Superlattice Coatings for Corrosion Resistant Applications, *Surf. Coat. Technol.*, 1999, **120–121**, p 535
13. J. Lin, J.J. Moore, B. Mishra, M. Pinkas, and W.D. Sproul, Nano-Structured CrN/AlN Multilayer Coatings Synthesized by Pulsed Closed Field Unbalanced Magnetron Sputtering, *Surf. Coat. Technol.*, 2009, **204**, p 936–940
14. Z.B. Zhao, Z.U. Rek, S.M. Yalisove, and J.C. Bilello, Nanostructured Chromium Nitride Films with a Valley of Residual Stress, *Thin Solid Films*, 2005, **472**, p 96
15. Z. Han, J. Tian, Q. Lai, X. Yu, and G. Li, Effect of N2 Partial Pressure on the Microstructure and Mechanical Properties of Magnetron Sputtered CrNx Films, *Surf. Coat. Technol.*, 2003, **162**, p 189
16. A. Barata, L. Cunha, and C. Moura, Characterisation of Chromium Nitride Films Produced by PVD Techniques, *Thin Solid Films*, 2001, **398–399**, p 501
17. C.-Y. Lin and F.-H. Lu, Oxidation Behavior of AlN Films at High Temperature Under Controlled Atmosphere, *J. Eur. Ceram. Soc.*, 2008, **28**, p 691
18. H.-Y. Chen and F.-H. Lu, Oxidation Behavior of Chromium Nitride Films, *Thin Solid Films*, 2006, **515**, p 2179
19. E. Fullerton and I. Schuller, Structural Refinement of Superlattices from X-Ray Diffraction, *Phys. Rev. B*, 1992, **45**, p 9292
20. J. Ning, S. Xu, K.N. Ostrikov, C. Jianwei, L. Yinan, K. Mei Ling, and S. Lee, Synthesis and Structural Properties of Al–C–N–O Composite Thin Films, *Thin Solid Films*, 2001, **385**, p 55
21. J.X. Zhang, H. Cheng, Y.Z. Chen, A. Uddin, Shu. Yuan, S.J. Geng, and S. Zhang, Growth of AlN Films on Si (100) and Si (111) Substrates by Reactive Magnetron Sputtering, *Surf. Coat. Technol.*, 2005, **198**, p 68
22. R. Katamreddy, R. Inman, G. Jursich, A. Soulet, A. Nicholls, and C. Takoudis, Post Deposition Annealing of Aluminum Oxide Deposited by Atomic Layer Deposition Using tris(diethylamino)aluminum and Water Vapor on Si(100), *Thin Solid Films*, 2007, **515**, p 6931
23. V.N. Antsiferov, V.G. Gilyov, and V.I. Karmanov, IR-Spectra and Phases Structure Of Sialons, *Vib. Spectrosc.*, 2002, **30**, p 169
24. L. Li, X. Hao, N. Yu, D. Cui, X. Xu, and M. Jiang, Low-Temperature Solvent Thermal Synthesis of Cubic AlN, *J. Cryst. Growth*, 2003, **258**, p 268
25. G. Shukla and A. Khare, Dependence of N2 Pressure on the Crystal Structure and Surface Quality of AlN Thin Films Deposited Via Pulsed Laser Deposition Technique at Room Temperature, *Appl. Surf. Science*, 2008, **255**, p 2057
26. K.P. Bhuvana, J. Elanchezhiyan, N. Gopalakrishnan, and T. Balasubramanian, Codoped (AlN) and Monodoped (Al) ZnO Thin Films Grown by RF Sputtering: A Comparative Study, *Appl. Surf. Science*, 2008, **255**, p 2026
27. A. Raveh, M. Weiss, M. Pinkas, D.Z. Rosen, and G. Kimmel, Graded Al–AlN, TiN, and TiAlN Multilayers Deposited by Radio-Frequency Reactive Magnetron Sputtering, *Surf. Coat. Technol.*, 1999, **114**, p 269
28. T. Suzuki, H. Saito, M. Hirai, H. Suematsu, W. Jiang, and K. Yatsui, Preparation of Cr(Nx,Oy) Thin Films by Pulsed Laser Deposition, *Thin Solid Films*, 2002, **407**, p 118
29. O. Banakh, P.E. Schmid, R. Sanjinés, and F. Lévy, High-Temperature Oxidation Resistance of Cr1−xAlxN Thin Films Deposited by Reactive Magnetron Sputtering, *Surf. Coat. Technol.*, 2003, **163–164**, p 57
30. M. Hirai, Y. Ueno, T. Suzuki, W. Jiang, C. Grigoriu, and K. Yatsui, Characteristics of (Cr1-x, Alx)N Films Prepared by Pulsed Laser Deposition, *Jpn. J. Appl. Phys.*, 2001, **40**, p 1056
31. J.E.B. Randles, Surface Tension of Dilute Acid Solutions, *Discuss. Faraday Soc.*, 1947, **1**, p 11
32. H. Schäfer and H.-R. Stock, Improving the Corrosion Protection of Aluminium Alloys Using Reactive Magnetron Sputtering, *Corros. Sci.*, 2005, **47**, p 953
33. J.M. Bastidas, M. Saiki, S.O. Rogero, I. Costa, and J.L. Polo, An Electrochemical Study of the Behaviour of Ear Piercing Studs Immersed in a Culture Medium, *J. Appl. Electrochem.*, 2002, **32**, p 487
34. W. Aperador, R. de Mejía Gutiérrez, and D.M. Bastidas, Steel Corrosion Behaviour in Carbonated Alkali-Activated Slag Concrete, *Corros. Sci.*, 2009, **51**, p 2027
35. M. Fenker, M. Balzer, H.A. Jehn, H. Kappl, J.-J. Lee, K.-H. Lee, and H.-S. Park, Improvement of the Corrosion Resistance of Hard Wear Resistant Coatings by Intermediate Plasma Etching or Multilayered Structure, *Surf. Coat. Technol.*, 2002, **150**, p 101
36. H.A. Jehn, Improvement of the Corrosion Resistance of PVD Hard Coating–Substrate Systems, *Surf Coat Technol.*, 2000, **125**, p 212
37. G. Bejarano, C.A. Rincon, W. Aperador, and J.C. Caicedo, Mejoramiento de la Resistencia a la Corrosión del Acero AISI, 4140 Utilizando Multicapas de Titanio/Nitruro de Titanio, *Rev. Fac. Ing. Univ. Antioquia*, 2008, **46**, p 7
38. H. Altun and S. Sen, The Effect of DC Magnetron Sputtering AlN Coatings on the Corrosion Behaviour of Magnesium Alloys, *Surf. Coat. Technol.*, 2005, **197**, p 193
39. W. Tato and D. Landolt, Electrochemical Determination of the Porosity of Single and Duplex PVD Coatings of Titanium and Titanium Nitride on Brass, *J. Electrochem. Soc.*, 1998, **145**, p 4173